Proof of Concept of a Novel Neck-Situated Wearable PPG System for Continuous Physiological Monitoring

Sukhpreet Singh, Michał Kozłowski, Irene García-López, *Student Member, IEEE*, Zhou Jiang, and Esther Rodriguez-Villegas, *Senior Member, IEEE*

***Abstract*— Continuous overnight vital signs monitoring would be ideal for patients suffering from epilepsy, where life-threatening hypoxemias can occur during sleep. However, the existing physiological monitoring systems suffer from limitations in terms of usability factors and/or limited information of the signals being acquired. The body location of the monitoring system is a crucial consideration, seldom addressed by the wider community. This article presents a proof-of-concept, neck-worn photoplethysmography system, which was developed and tested to assess the feasibility of the neck as a monitoring site for longitudinal sensing of cardiac and respiratory responses during sleep. The novel system was compared against a gold-standard commercial multichannel cardiorespiratory polysomnography (PSG) system during oxygen desaturation cycles, to assess its ability to measure heart rate, respiratory rate (RR), and peripheral blood oxygen saturation (SpO_2) on 15 participants. The findings for heart rate showed a marginal mean error of 0.47 beats/min with limits of agreement (LOA) at 95% confidence between −3.17 and 4 bpm. RR comparisons had an overall mean error of 0.43 breaths/min, with LOA at 95% confidence between −2.73 and 3.3 bpm. Lastly, the system accurately outputs SpO_2 with an overall root-mean-square error of 1.44% between 90 and 100% SpO_2 using a custom calibration method. Moreover, it was observed that the neck made it possible for the system to detect desaturation events on an average 12.6 s prior to the PSG system, which used a peripheral finger-based PPG system. Ultimately, this proof-of-concept study illustrates the viability of neck-based sensing for minimally invasive monitoring of cardiac and respiratory vitals during sleep.**

***Index Terms*— Biomedical monitoring, epilepsy, photoplethysmography (PPG), pulse oximetry, wearable sensors.**

I. Introduction

EPILEPSY is a neurological condition affecting the central nervous system, resulting in bursts of electrical activity in the brain, resulting in seizures with a variety of physical and/or cognitive manifestations [1]. The disease affects more than 500 000 people in the U.K. and 50 million worldwide [2]. It is unclear, in most cases, as to what causes epilepsy—possible causes include a stroke, severe head injury, or drug abuse [1].

Epileptic events during sleep, or nocturnal seizures, can lead to hypoxemic events and potentially be accompanied by central apneas in the ictal phase [3], [4]. This results in nocturnal seizures having an increased risk of mortality caused by sudden unexpected death in epilepsy (SUDEP) [5]–[7]. Although the exact mechanisms of SUDEP are uncertain, cardiac and respiratory impairment and ictal phase hypoxemic events have shown to be potentially relevant factors [3], [8]–[10]. The risk of SUDEP affects people of all ages [11]. Hence, having easy-to-use, unobtrusive systems that allows for long-term monitoring of epilepsy patients during sleep could potentially help to reduce the risk of SUDEP.

Currently, the gold standard for epilepsy patient monitoring involves a video-based electroencephalogram (EEG) or multichannel cardiorespiratory polygraphy/polysomnography (PSG) for epilepsy [12], [13]. A variety of physiological channels are sensed, which might include electroencephalography (EEG), photoplethysmography (PPG), electrocardiography (ECG), electromyography (EMG), and respiratory effort.

Despite PSG and video-based EEG systems showing their versatility in overnight diagnostic studies and/or in-clinic long-term monitoring, these systems are designed with supervised clinical use in mind. Thus, they are not ideal for long-term, ideally unsupervised, monitoring of the cardiorespiratory function of the patient [12], [13]. The potential wearable technologies could offer in this context is hence becoming increasingly apparent [14]–[18].

Over the last few decades, the increased commercialization of PPG-based wearable devices has been evident, garnering considerable market share and press coverage. The devices for pervasive health and fitness monitoring, such as the Fitbit (Fitbit Inc., California, USA) or the Apple watch (Apple Inc., California, USA), make use of PPG as one of their main physiological sensors due to its noninvasive nature, simplicity, and small form factor [19].

Despite offering a high degree of convenience and usability compared to conventional clinical health monitors, these systems are not regulated as medical devices for physiological monitoring purposes. This is unlikely to change in the future, due to, among other reasons, the limitations associated with the signal acquisition in the chosen body location [20], [21].

Manuscript received February 19, 2021; revised April 11, 2021; accepted April 26, 2021. Date of publication May 26, 2021; date of current version June 10, 2021. This work was supported by the European Research Council (ERC) under Grant 724334. The Associate Editor coordinating the review process was Dr. Subhas Chandra Mukhopadhyay. *(Corresponding author: Sukhpreet Singh.)*

The authors are with the Wearable Technologies Laboratory, Department of Electrical and Electronic Engineering, Imperial College London, London SW7 2BT, U.K. (e-mail: ss7719@ic.ac.uk).

Digital Object Identifier 10.1109/TIM.2021.3083415

Many anatomical positions have been suggested for PPG, the benefit of each of them being ultimately dependent on the intended purpose of the device. The neck, however, has conventionally not been chosen as a potential location for PPG sensing since other positions in the body are anatomically more suitable. However, those conventional locations are unsuitable to sense airflow, which in the context of high-risk intended uses is important to identify full central apneas. The neck offers the possibility of potentially monitoring both oxygen saturation levels and airflow [22].

Previous work using neck-based PPG has been very limited, only demonstrating the feasibility of extracting signals [23]–[25], characterizing the waveform [26], and analyzing potential artifacts and exploring the optimal location [24], [27]. This article advances the state of the art by presenting for the first time a proof of concept of a wearable system for PPG signal acquisition, together with analysis algorithms for extraction of heart rate (HR), respiratory rate (RR), and peripheral oxygen saturation (SpO_2).

II. Methods

A. Hardware

A custom PCB was designed to house an integrated PPG sensor (MAX30102, MAXIM integrated), which emits red (650–670 nm) and IR (870–900 nm) light, paired with a photodiode to quantify light absorption. The MAX 30102 was chosen due to its low-power capabilities; operating at 1.8 V and 3.3 V for the LEDs [28]. Furthermore, the small form factor (5.6 mm × 3.3 mm × 1.5 mm), programmable parameters, and built-in ambient light rejection make it practical for wearable applications [28]. A three-axis linear accelerometer (LIS2DH12, ST Electronics) was included to evaluate the activity and remove motion artifacts as necessary. The chosen accelerometer (LISDH12) specifically is ideal for wearable applications due to its low-power modes, high precision, and small form factor [29]. An NRF5232 microcontroller (Nordic Semiconductor) was used to acquire sensor data via a two-wire interface (TWI). The microcontroller is based on a 64-MHz Arm Cortex-M4 CPU, with 512-kb and 64-kb storage for flash and RAM, respectively [30]. Furthermore, this microcontroller supports the Bluetooth low energy (BLE) protocol for controlling wireless sensor data transmission. Data from the NWPPGS were transmitted wirelessly using a 2.4-GHz mini-antenna (2450AT18b100, Johanson Technology, Inc.). A custom rechargeable 80 mAh, 3.8-V lithium ion polymer battery supplied power to the system, and was chosen for its capacity and small form factor (20 mm × 16 mm × 4 mm). Voltage regulators were used to tune the voltage for each module to match the datasheet requirements (3.3 V for the microcontroller, accelerometer, and PPG sensor LED, and 1.8 V for the PPG sensor integrated circuit). Furthermore, power management circuitry was included to allow the battery to charge via a micro-USB cable. The custom PCB was housed in an additive manufactured enclosure to interface the sensor system with the suprasternal notch. In order to maximize the surface contact area between the complete Neck Worn PPG System (NWPPGS) and the suprasternal notch, a slight protruding feature was implemented in the bottom of the enclosure. A 0.2-mm acrylic screen was placed above the PPG sensor to fully enclose the inside circuitry. The overall dimensions of the physical enclosure were 28 mm × 28 mm × 10 mm. To allow for a more consistent pressure distribution across participants, a double-sided adhesive was used to bond the NWPPGS to the user.

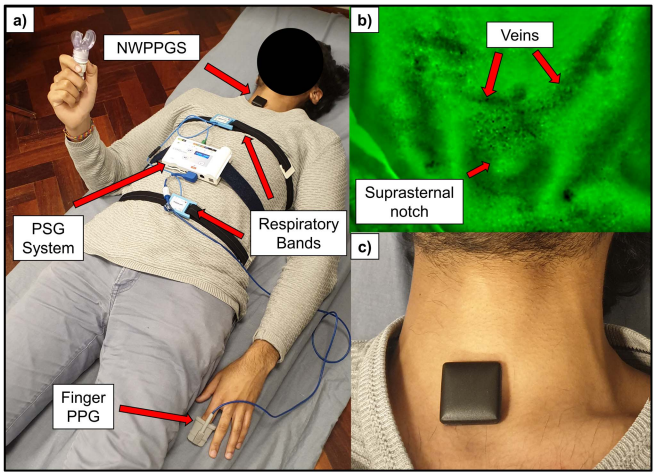

Fig. 1. (a) A study participant equipped with the SOMNOScreen PSG (respiratory bands and a finger PPG sensor) and the NWPPGS. (b) IR camera image showing the venous system near the suprasternal notch. The darker regions indicated by the red arrows show veins in the neck region. (c) NWPPGS system is equipped on a test subject using a double-sided adhesive.

B. Experimental Setup

Collecting PPG data with the NWPPGS was approved by an institutional review board: Local Ethics Committee of Imperial College London (ICREC ref.: 18IC4358). The study involved 15 healthy participants (ten male and five female), with an average age of 27 ± 2 years, an average body mass index (BMI) of 23.80 ± 3.57 kg/m^2, and a variety of skin colors. Recordings were captured with participants lying down in a dark room to mimic sleeping environments. This was carried out to simulate the device's aim of being utilized in bed at night. An IR camera was used to identify venous presence near the suprasternal notch, as shown in Fig. 1(b). If a heavy venous presence near the suprasternal notch was evident, the PPG sensor would be repositioned nearby to avoid venous architecture. Fig. 1(c) shows the NWPPGS applied to the suprasternal notch using a double-sided adhesive. Relevant channels of a portable PSG (SOMNOScreen and SOMNOmedics) system were used as a reference gold standard, namely transmission finger-based oximeter and thorax and abdomen respiratory bands. The complete setup of sensing devices can be seen in Fig. 1(a).

Raw data from the NWPPGS were sampled at 75 Hz. The SOMNOScreen system displayed HR and SpO_2 using four-beat averages. Data from the NWPPGS were transmitted via Bluetooth 5 to an in-house developed iOS app, with the minimum and maximum connection intervals between the NWPPGS and the tablet to be 20 and 40 ms, respectively. Lastly, data from the tablet were uploaded to a cloud-based

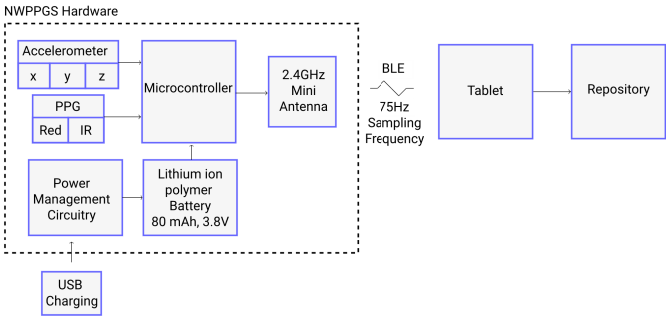

Fig. 2. Block diagram outlining the internal structure of the NWPPGS. Data are then transmitted from the NWPPGS to a tablet via BLE at 75 Hz, and then to a cloud-based repository for data analysis.

repository for analysis, as shown in Fig. 2. Manual markers were inputted on the SOMNOScreen and tablet for synchronization at the start of each experiment. Participants were first asked to breathe normally for 2 min, then wear a commercial respiratory modulating device designed to simulate high altitude (Ultrabreathe [31]) for 30–180 s. The respiratory modulating device safely limited air intake to allow for a controlled SpO_2 decrease. Each test involved four desaturation intervals, and two tests were taken from each user, resulting in eight total desaturation events. Manual markers were recorded on the tablet to indicate the start and end of every desaturation event to determine the delay in SpO_2 readings observed from both sensing modalities.

C. Signal Processing

The overall aim of the work was to quantify the feasibility to extract HR, RR, and SpO_2 from neck PPG signals, comparing their accuracy with respect to the same ground-truth parameters. The PPG signals acquired with the wearable system were processed as shown in Fig. 3. This is further described in subsequent sections.

1) Preprocessing: Data acquired from the SOMNOScreen and the NWPPGS were synchronized in time to ensure complete correspondence between samples. This was carried out automatically using cross-correlation between the acceleration reported from the NWPPGS accelerometer and chest band data. This synchronization was validated by confirming the time difference between the manual marker input between the SOMNOScreen and NWPPGS empirically. All data were subsequently downsampled to 15 Hz before undergoing analysis. Outlier data were removed by computing the magnitude of the accelerometer signal. The signal was separated into "usable" periods of relatively noise-free data and noisy time spans. After normalizing the amplitude of x-, y-, and z-directions, the magnitude of the acceleration was computed. Data segments were removed if the magnitude was larger than two standard deviations from the mean. This is exemplified in Fig. 4—the black and red periods of the data are the "usable" and "noisy" segments, after masking the data using accelerometer data, respectively. The binary mask was smoothed to produce homogeneous, nondiscontinuous data for analysis.

Fig. 5 shows raw signals for both the red and IR lights in the NWPPGS. Cardiac components of the PPG signals

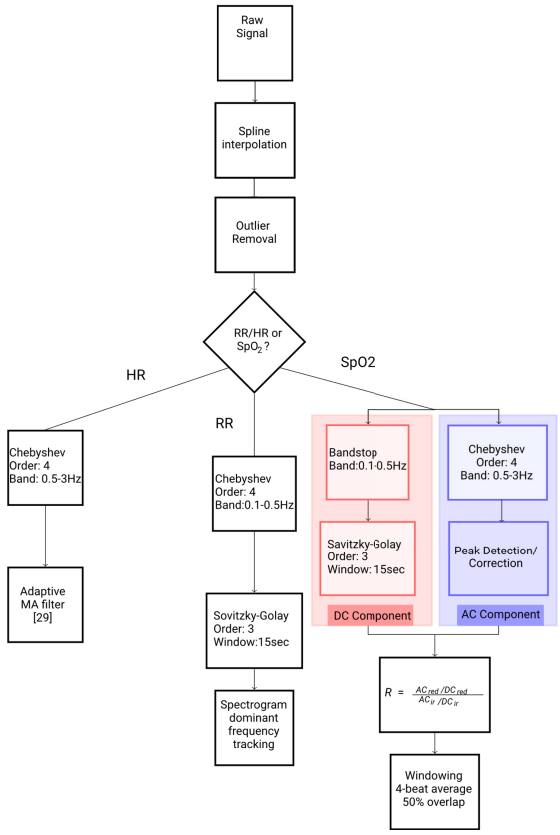

Fig. 3. Flow diagram illustrating the signal processing methodology undergone by both the red and IR PPG signals. The data underwent spline interpolation to downsample the data to 15 Hz, and then next to an outlier detection/removal stage. Lastly, distinct signal processing pipelines were applied depending on whether RR, HR, or SpO_2 were computed.

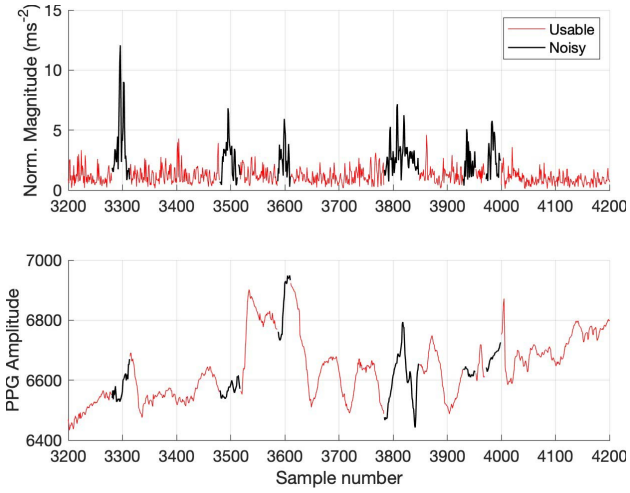

Fig. 4. Example of data showing interference with motion artifacts. Normalized accelerometer signal (above) and red LED signal (below). Black lines illustrate y periods of the interference caused by the movement of artifacts as determined by the masking step.

are difficult to fully interpret in this signal due to the large influence of respiratory-induced signal modulations during breathing. To this end, unique filtering techniques were used depending on whether a respiratory or a cardiac marker was being investigated.

2) RR Processing: To analyze the respiratory components of the signal, a fourth-order Chebyshev filter was applied

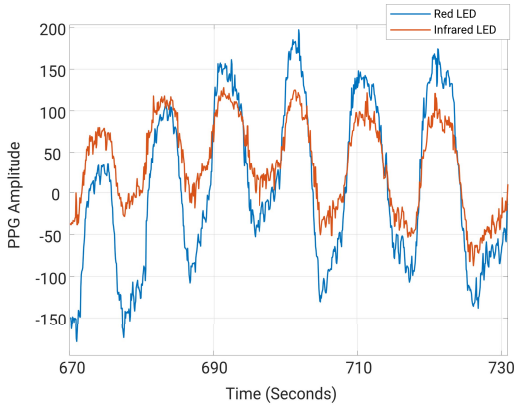

Fig. 5. Example displaying the ac components of the PPG signals acquired from the NWPPGS, including the larger respiratory waveforms, with the smaller cardiac pulses embedded in the respiratory component of the signal for both the red LED (blue) and IR LED (orange).

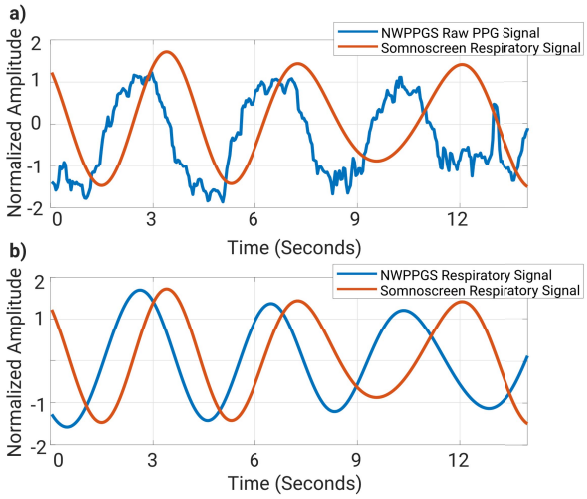

Fig. 6. (a) Unfiltered red LED PPG signal from the NWPPGS (blue) and the respiratory output from the SOMNOScreen respiratory bands (orange). Both signals are synchronized in time. (b) Filtered red LED PPG signal to isolate the respiratory component of the signal (blue) and the respiratory output calculated from the SOMNOScreen system (orange).

across the raw PPG signals, in order to isolate frequencies in the respiratory band (0.1–0.5 Hz, 6–30 breaths/min). A third-order Savitzky–Golay filter was then used to smooth the signal of any sharp/transient signal artifacts which were still evident in the signal after bandpass filtering. The SOMNOScreen system quantified respiratory effort, as the thorax and abdomen contracted during breathing; however, RR was not provided by the SOMNOScreen system. Fig. 6 shows the sum of the thoracic and abdominal signal obtained from the SOMNOScreen, superimposed on the raw red light PPG signal [Fig. 6(a)], and the filtered respiratory component of the signal [Fig. 6(b)]. Therefore, to determine the RR, dominant frequencies of each signal were tracked using the built-in MATLAB function tfridge(). This outputted the largest energy ridge in the time-frequency spectrum, and thus isolated the dominant frequency over time. This RR algorithm was applied to both sensing modalities for comparison. The total amount of respirations/breaths taken by each subject was tallied to verify the ability of the NWPPGS to identify respiration cycles to that of the SOMNOScreen respiratory bands. This was carried out using the MATLAB function findpeaks() with thresholding.

3) HR Processing: To remove any bias caused by respiration and to isolate the cardiac band, a fourth-order Chebyshev filter (0.5–3 Hz) was applied across the signal. A frequency tracking-based HR algorithm was used for its low computational complexity. This method estimated HR using an oscillator-based adaptive notch filter algorithm which tracked the dominant frequencies of the signal [32], [33].

4) Blood Oxygen Saturation Processing: As shown in Fig. 3, to derive the SpO_2 signal, the ac and dc components of the signal needed to be isolated reliably first. A bandstop was applied between 0.1 and 0.5 Hz for both the red and IR PPG signals to remove the respiratory component. Next, the signal was processed through a third-order Savitzky–Golay filter to construct the dc signal.

The ac component of the signal was determined by first localizing the peaks and valleys of the signal using the findpeaks() MATLAB function. Due to the possibility of false identification of nearby peaks, a peak correction step was introduced by creating a sample window at the calculated peak equal to half the sampling frequency. This ensured that the chosen peak was the maximum and the valley was the minimum. In order to match the SOMNOScreen system, a four-beat average window was implemented to calculate the SpO_2.

Calibration of the system was carried out in line with the PPG sensor manufacturer's calibration guidelines [34]. Further analytical steps were required, since only a subset of subjects experienced a desaturation event greater than 5%. Therefore, to apply equal weights to all $SpO_2(\%)$ levels, a k-nearest neighbor ($k$nn) search algorithm was used. The algorithm chose the k closest points to the mean of each SpO_2 percentage, to balance the number of observations. The common number of neighbors used for all percentages was equal to the number of samples received for the lowest SpO_2 level of 90%. Fig. 7 shows a scatter plot displaying the formed linear regression of the reference SpO_2 values against the corresponding processed R ratios for all subjects.

The observations falling within one standard deviation ($R_{\text{obs}} \in \mu \pm \sigma$) are displayed in blue and the $k$nn surrounding the mean in yellow. A linear model was fit to the data by least-squares approximation, i.e., by minimizing the squared distance between each observation and the regression line. The resulting linear function for SpO_2

$$SpO_2 = 107.07 - 9.42R. \tag{1}$$

This provided the neck calibration coefficients of $A = 107.07$ (intercept of the regression line) and $B = 9.42$ (slope of the regression line). The coefficient of determination (r^2) demonstrated that the proposed model significantly ($p < 0.001$) explained 90% of the SpO_2 variance.

III. Results

A. Evaluation Criteria

The Bland–Altman and scatter plots were used to assess the agreement between the NWPPGS and SOMNOScreen for

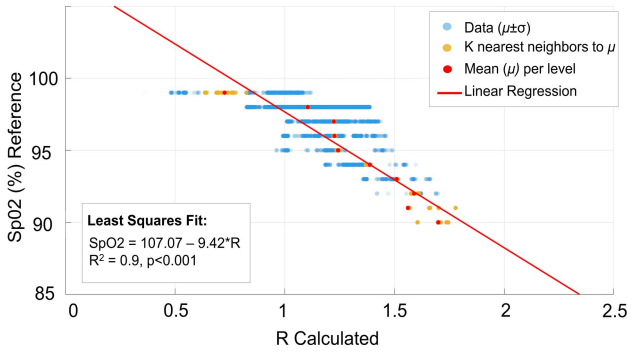

Fig. 7. Custom regression curve to determine SpO_2 from the NWPPGS. The blue dots represent the R calculated values for each SpO_2 level with a set of transparency factors; therefore, regions with increased density of points appear in dark blue. The yellow dots represent the $k$nn closest points which were used to influence the linear regression curve, and thus the equation.

HR, RR, and SpO_2. Root-mean-square error (RMSE) was calculated to quantify the absolute prediction error of RR, HR, and SpO_2 for each test subject j, given by

$$\text{RMSE}_j = \sqrt{\frac{\sum_{i=1}^{N}(y_i - \hat{y}_i)^2}{N}} \tag{2}$$

where $(y_i - y_b i)^2$ corresponds to the residuals and N represents the total number of samples. The overall RMSE (ORMSE) was then obtained by averaging individual RMSE_j for all subjects based on the sample size for each subject.

B. Respiratory Rate

Fig. 8(a) shows a sample RR response for both the SOMNOScreen and NWPPGS. Due to the stable conditions of the study, the range of RRs examined was between 10 and 18 breaths/min (bpm). The calculated ORMSE of RR was 1.72 bpm when comparing the NWPPGS system and the SOMNOScreen. Fig. 8(b) shows the Bland–Altman and scatter plots for RR between the NWPPGS system and SOMNOScreen. The value of μ was quantified by computing the average of all HR discrepancies. The limits of agreement (LOA) at a 95% confidence showed a mean error of $\pm 1.96 \times \sigma$. A mean bias of 0.43 bpm was obtained in the Bland–Altman plot shown in Fig. 8, with the upper and lower LOA being 3.3 and -2.7 bpm, respectively. A positive sloping bias was observed in the Bland–Altman plot, indicating that higher calculated RRs for the NWPPGS were overestimated, and lower calculated RRs were underestimated. The coefficient of determination (r^2) for RR demonstrated that the proposed model significantly explained 68% of the RR variance between SOMNOScreen and NWPPGS. The average cumulative respiration count per user was estimated as 177.2 respirations with a standard deviation of 48.9 respirations and 181.6 respirations with a standard deviation of 49.4 respirations for the PPG and SOMNOScreen system, respectively. The NWPPGS recorded 97.6% of the total respirations recorded by the SOMNOScreen.

C. Heart Rate

Fig. 9(a) shows a similar HR response between both systems. The experimental HR range was between 43 and

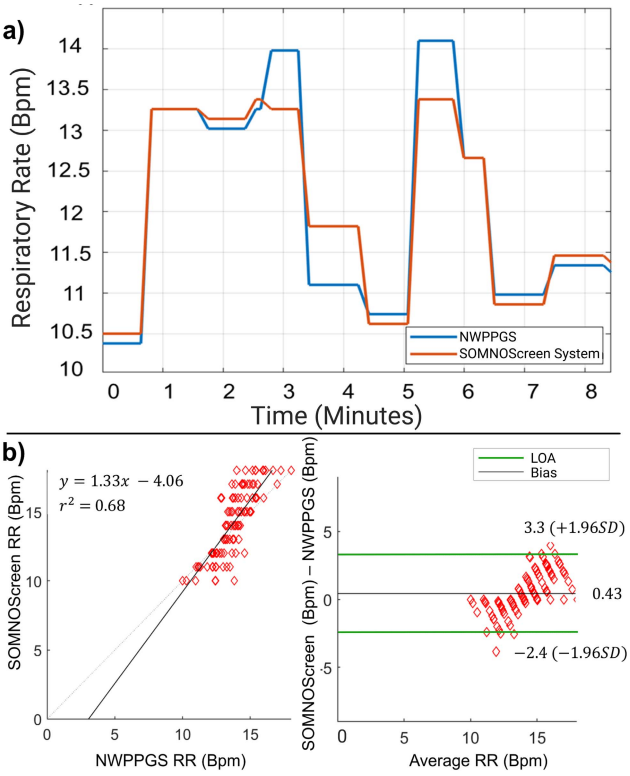

Fig. 8. (a) Calculated RRs from both the NWPPGS (blue) and the SOMNOScreen (orange), both synchronized in time. (b) Linear regression (left) and Bland–Altman plot (right) showing the comparison between RRs automatically extracted from the NWPPGS and the reference test, SOMNOScreen. LOA of the Bland–Altman plot at 95% confidence were 3.3 and -2.4 bpm for the upper and lower bound, respectively.

96 beats/min (bpm). Fig. 9(b) shows a scatter plot and a Bland–Altman plot used to compare the measured HR of the NWPPGS method with the ground-truth SOMNOScreen. A mean bias of 0.47 bpm was obtained, with the upper and lower LOA bounds being 4 and -3.1 bpm, respectively, at a 95% confidence interval. The bias line shows that the error is consistent between the HR levels, and is not adversely affected by varying bpm levels. The scatter plot between both modalities showed a high degree of agreement, with r^2 of 95%. Finally, the NWPPGS yielded an ORMSE of 1.69 bpm.

D. Blood Oxygen Saturation

Once the PPG device was calibrated, the ability of this device to estimate SpO_2 could be evaluated. A leave-one-subject-out cross-validation (LOSO-CV) strategy assessed the performance of the proposed linear model. For that, one test subject was removed from the whole set iteratively to repeat the linear regression fitting with the rest of the subject's data. The calculated R values of the test subjects were then inputted in the calibrated model to derive the corresponding SpO_2 levels. The RMSE and ORMSE were additionally calculated to quantify the prediction error.

The LOSO-CV method confirmed the estimation of SpO_2 values, with a very low absolute error of ORMSE $=$ 1.44%. Generic coefficients given by the PPG sensor manufacturer resulted in an ORMSE $=$ 12.54%, which is much larger

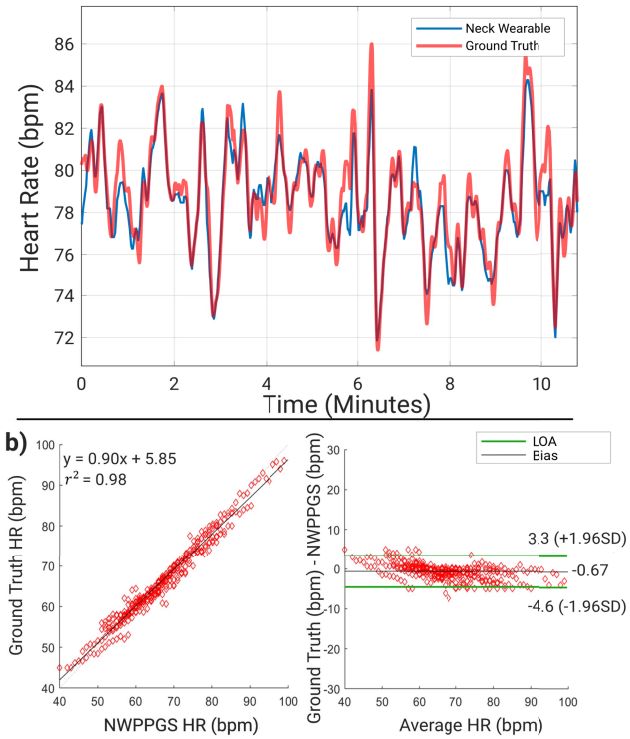

Fig. 9. (a) Sample HR response from both the NWPPGS (blue) and SOMNOScreen (orange), both synchronized in time. (b) Linear regression (left) and Bland–Altman plot (right) used to compare HR from the NWPPGS and SOMNOScreen. LOA of the Bland–Altman plot were 3.3 and −4.6 bpm for the upper and lower bounds, respectively, with a 95% confidence interval.

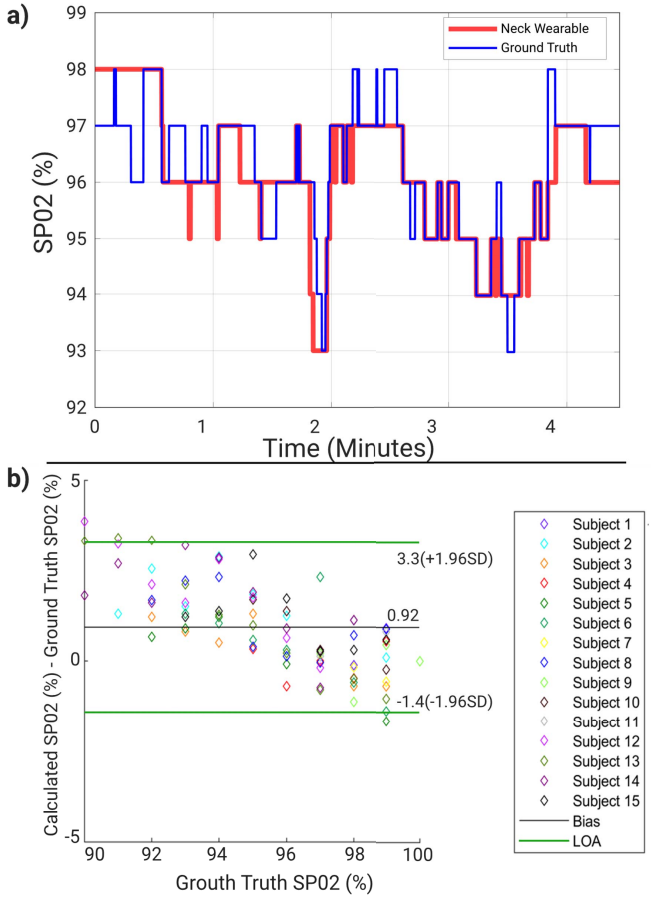

Fig. 10. (a) SpO_2 output from the NWPPGS (blue) and SOMNOScreen (red). (b) Bland–Altman plot (right) used to compare SpO_2 with the NWPPGS and SOMNOScreen. LOA of the Bland–Altman plot were 3.3% and −1.4% for the upper and lower bounds, respectively, at a 95% confidence interval. A negative bias is visually noticeable in the plot with overestimated values at lower SpO_2 levels.

than the obtained 1.44%, showing the need for custom calibration. Fig. 10(a) shows desaturation events occurring with the SpO_2 response of both systems synchronized. Clearly, the NWPPGS responded appropriately to desaturation events. Fig. 10(b) shows the Bland–Altman plot comparing the SpO_2 calculated by the NWPPGS and the ground-truth SpO_2 from the SOMNOScreen system. The mean bias of 0.92% was observed, with LOA of 3.3% and −2.4% for the lower and higher bounds, respectively, at a 95% confidence interval. A negatively trending slope was evident, as the error margins increased for lower SpO_2 levels. It was understood that lower SpO_2 levels slightly overestimated SpO_2 values. However, the NWPPGS system produced very promising results for resting-state SpO_2 levels. Lower SpO_2 had a far smaller density of data points compared to higher SpO_2 levels, as can be seen in Fig. 7.

The BMI and age of each subject were tabulated along with the RMSE for each test in Table I. No significant correlation was found between BMI of subjects and RMSE.

Lastly, the time lag between the SpO_2 outputs with respect to the manually marked start of events was also compared, for both the NWPPGS method and the SOMNOScreen ground truth. Fig. 11 shows the outline of the overall time delay associated with both the NWPPGS and SOMNOScreen ability to respond to desaturation events. The mean delay was 15.01 and 27.29 s, with standard deviations of 3.31 and 6.13 s for the NWPPGS and SOMNOScreen system, respectively. Hence, it was found that the NWPPGS responded to desaturation

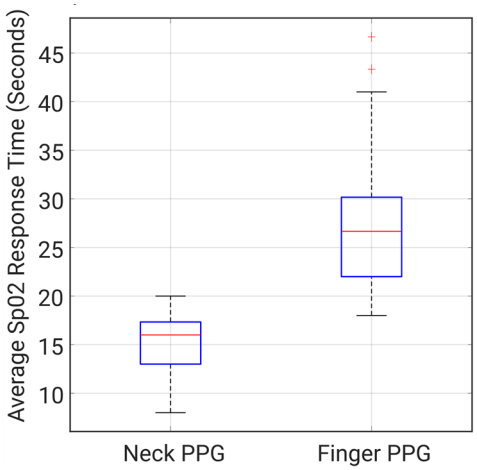

Fig. 11. Boxplots explaining the mean time for each sensing modality to respond to a desaturation event per user. The error bars correspond to the standard deviation.

changes on an average of 12.28 s prior to the ground-truth SOMNOScreen system.

IV. Discussion

This article demonstrates for the first time that it is possible to extract SpO_2 values from a neck-based wearable

TABLE I
SpO_2 RMSE, AGE, AND BMI FOR EACH USER ACROSS BOTH TESTS

User No.	RMSE - Test 1 (%)	RMSE - Test 2 (%)	BMI (kg/ m^2)	Age (Years)
1	0.95	0	20.8	23
2	0.47	1.58	24.2	31
3	0	1.17	26.2	29
4	0.24	0.95	23.8	32
5	0.76	0.91	28.2	28
6	0.53	0.56	24.3	26
7	0.19	0.76	26.5	27
8	0.76	0.91	32.9	28
9	0.87	1.77	21.2	31
10	0.45	0.48	20.3	25
11	0.56	0.52	23.7	28
12	3.1	1.15	18.9	27
13	1.57	0.81	22.6	29
14	1.93	1.43	22.7	28
15	0.64	1.01	20.1	28

RMSE of 0 (%) occurred for two tests that had no desaturation (Run 1 – User 3, and Run 2 – User 1)

device with accuracies that could match acceptable regulatory margins [35], while also having the possibility of obtaining respiratory and heart rates from only the sensed PPG signal. Furthermore, it was demonstrated that desaturations manifested on the signal acquired with the novel wearable system from the neck were 12.6 s faster, on average, than when sensing the PPG signal with the finger. Although faster responses have been reported from other anatomical positions before [36], [37], the neck is still significantly faster than the finger. This response can be crucial when trying to develop a monitoring system intended to be used in critical applications—such as the prevention of SUDEP [3], [9].

The evaluation results, however, showed that the SpO_2 error increased at lower recorded SpO_2 levels. This error can be attributed to the difficulty of obtaining a homogeneous distribution of SpO_2 levels with the current experimental setup, especially at lower SpO_2 levels between 90% and 94%. The SpO_2 desaturation levels were not consistent across participants, as each participant equipped the respiratory modulating device for an amount of time that they found comfortable. The feasibility has been proven, prompting the need for future controlled hypoxia experiments, involving a larger number of subjects, a wider range of demographic characteristics, lower desaturations, and less controlled conditions. Those will allow for a more precise tuning of the custom calibration parameters. Moreover, extraction of the ac and dc values for estimation of the SpO_2 was limited by the presence of noise. Although this was mitigated using accelerometer-based thresholding, bandpass filtering, and outlier removal, ideally a more elaborate automatic signal processing algorithms could be developed in future work [38]–[41].

In terms of RR, the system was able to reliably identify 97.6% of the total respirations recorded by the ground-truth system. This result can be presumed to be preliminary, since the cohort of subjects and RRs were limited; it is nevertheless encouraging, since it demonstrates the potential of the approach for analyzing respiratory activity from the neck-acquired PPG signal. In a clinical context, this may be of use to further support decisions from additional sensing modalities [22] when trying to identify potentially dangerous apneas, or even apnea events in the ictal phase [4], [42]. Additional work could be carried out to investigate the optimal shape and location of the enclosure, potential customization for the user, and/or even the creation of variants for typical anatomical characteristics. This is because the shape of the suprasternal notch varies between subjects, with some having a considerably higher degree of curvature than others. For subjects with more concave suprasternal notches, the wearable could benefit from having a smaller form factor or a more ergonomic shape to increase the contacting surface area between the sensor and the user. Additionally, it has been reported that the mechanism for respiration involves two degrees of freedom, namely the thorax and abdomen [43]. It is likely that the NWPPGS is more heavily influenced by the movement of the thorax and it would be worth investigating if results from subjects with abdomen-dominant breathing are as accurate using the NWPPGS. Furthermore, the current experimental setup tested RRs in a resting state. Further experimentation should consider a wider range of RRs, introduce apneic events, and investigate whether using PPG in combination with airflow sensing could increase the accuracy of the latter in differentiating potentially dangerous apneas/hypopneas, prior to developing a more advanced prototype incorporating both sensing modalities to be tested in patients. The range of HR measured from 40 to 100 bpm in healthy individuals showed a strong correlation and low degree of error that are sufficiently encouraging to support further investigation into the use of the PPG signal sensed in the neck. A potential study could obtain HR at real time to support other biomarkers in a variety of clinical applications. The Bland–Altman plot showed that errors did not increase with an increase or decrease in HR. This is shows a potential of this system to detect unusual transitory cardiac trends in the context of epilepsy during seizures and postictal states [1]. HR information, together with SpO_2 estimation, and airflow [22] could help to increase the accuracy in the interpretation of dangerous overnight apnea events [9]. However, as with RR and SpO_2, future work needs to be carried out to confirm the robustness of the approach in a larger cohort of subjects with wider demographic characteristics and less controlled conditions. We have used the real-time transmission of all data with offline processing to demonstrate the proof of concept. However, different architectures are possible depending on the chosen application. For example, in cases where the recorded physiological parameters are only needed during a consultation with a doctor, continuous transmission between the NWPPGS and the tablet can be triggered for small periods overnight, keeping the system in low power mode at other times, thereby saving battery life. Additionally, the NWPPGS could transmit data on request, which could be visualized and assessed either on a tablet or a cloud-based system. This, however, comes with the disadvantage of reduced battery life. Alternatively, the parameters could be computed on the

NWPPGS itself, and transmission will be triggered only when abnormal values are detected. An on-device alarm system in the presence of abnormal values may be advantageous in future iterations to decrease its monitoring reliance on the tablet in the event connection is lost. Ultimately, the different modes can be used together to optimize the power consumption of the system depending on the use case. Therefore, further investigation is required to assess the feasibility of which parameters can be calculated on the NWPPGS itself, and to adjust data transfer rates between the NWPPGS and the tablet to optimize for battery life and parameter detection time.

An additional challenge to optimizing battery life for wearable applications is the time delay generated during data transmission. The NWPPGS's maximum connection interval between the tablet and NWPPGS was set to 40 ms—it can therefore be assumed that this delay between the sensed parameter from the NWPPGS being transmitted to the tablet would be of little consequence for real-time continuous data transfer and analysis.

V. Conclusion

Noninvasive real-time sleep monitoring of patients can be beneficial to aid in the fast identification of potentially life-threatening physiological states in certain clinical contexts, such as for SUDEP prevention. In this article, we demonstrated the viability of extracting typical cardiorespiratory parameters using a wearable PPG-based approach on the neck. The feasibility of extracting blood oxygen saturation, pulse, and respiration rate is demonstrated in a pilot study evaluation comparing the outputs of the developed custom algorithms applied to the sensed signal when compared to the measurements obtained using signals recorded with a typical commercial cardiorespiratory multichannel device. It was also proven that the novel wearable responded to desaturation events quicker than the gold-standard finger oximetry approach. This would be an important advantage when trying to develop an alarm device for time-critical applications, such as SUDEP.

Acknowledgment

The authors kindly acknowledge Acurable for providing the necessary hardware for the designed wearable system. They declare no conflict of interest. They also acknowledge Dr. Syed Anas Imtiaz for his troubleshooting and embedded systems assistance.

References

[1] WHO. (2019). *Epilepsy*. [Online]. Available: https: //www.who.int/en/news-room/fact-sheets/detail/epilepsy

[2] WHO. (2019). *WHO—Epilepsy: A Public Health Imperative*. [Online]. Available: http://www.who.int/mental health/neurology/epilepsy/report 2019/en/

[3] V. Latreille *et al.*, "Nocturnal seizures are associated with more severe hypoxemia and increased risk of postictal generalized EEG suppression," *Epilepsia*, vol. 58, no. 9, pp. e127–e131, Sep. 2017.

[4] L. Nashef, F. Walker, P. Allen, J. W. Sander, S. D. Shorvon, and D. R. Fish, "Apnoea and bradycardia during epileptic seizures: Relation to sudden death in epilepsy," *J. Neurol., Neurosurg. Psychiatry*, vol. 60, no. 3, pp. 297–300, Mar. 1996.

[5] D. J. Thurman, D. C. Hesdorffer, and J. A. French, "Sudden unexpected death in epilepsy: Assessing the public health burden," *Epilepsia*, vol. 55, no. 10, pp. 1479–1485, Oct. 2014.

[6] A. G. Holst *et al.*, "Epilepsy and risk of death and sudden unexpected death in the young: A nationwide study," *Epilepsia*, vol. 54, no. 9, pp. 1613–1620, Sep. 2013.

[7] D. M. Ficker *et al.*, "Population-based study of the incidence of sudden unexplained death in epilepsy," *Neurology*, vol. 51, no. 5, pp. 1270–1274, Nov. 1998.

[8] O. Devinsky, "Sudden, unexpected death in epilepsy," *New England J. Med.*, vol. 365, no. 19, pp. 1801–1811, Nov. 2011.

[9] O. Devinsky, D. C. Hesdorffer, D. J. Thurman, S. Lhatoo, and G. Richerson, "Sudden unexpected death in epilepsy: Epidemiology, mechanisms, and prevention," *Lancet Neurol.*, vol. 15, no. 10, pp. 1075–1088, Sep. 2016.

[10] P. Ryvlin *et al.*, "Incidence and mechanisms of cardiorespiratory arrests in epilepsy monitoring units (MORTEMUS): A retrospective study," *Lancet Neurol.*, vol. 12, no. 10, pp. 966–977, Oct. 2013.

[11] C. Jy, "Late-onset epilepsy associated with untreated obstructive sleep apnea: A case report and literature review," *Neurol. Disorders Therapeutics*, vol. 2, no. 2, pp. 1–5, Apr. 2018.

[12] S. V. Jain, T. Dye, and P. Kedia, "Value of combined video EEG and polysomnography in clinical management of children with epilepsy and daytime or nocturnal spells," *Seizure*, vol. 65, pp. 1–5, Feb. 2019.

[13] M. A. Tork *et al.*, "Sleep pattern in epilepsy patients: A polysomnographic study," *Egyptian J. Neurol., Psychiatry Neurosurg.*, vol. 56, no. 1, pp. 1–5, Dec. 2020.

[14] K. Vandecasteele *et al.*, "Automated epileptic seizure detection based on wearable ECG and PPG in a hospital environment," *Sensors*, vol. 17, no. 10, p. 2338, Oct. 2017.

[15] M. Ghamari, "A review on wearable photoplethysmography sensors and their potential future applications in health care," *Int. J. Biosensors Bioelectron.*, vol. 4, no. 4, p. 195, 2018.

[16] E. L'Her, Q.-T. N'Guyen, V. Pateau, L. Bodenes, and F. Lellouche, "Photoplethysmographic determination of the respiratory rate in acutely ill patients: Validation of a new algorithm and implementation into a biomedical device," *Ann. Intensive Care*, vol. 9, no. 1, p. 11, Dec. 2019.

[17] J. Allen, "Photoplethysmography and its application in clinical physiological measurement," *Physiol. Meas.*, vol. 28, no. 3, pp. R1–R39, Mar. 2007.

[18] I. García-López and E. Rodriguez-Villegas, "Extracting the jugular venous pulse from anterior neck contact photoplethysmography," *Sci. Rep.*, vol. 10, no. 1, pp. 1–12, Dec. 2020.

[19] T. Tamura, Y. Maeda, M. Sekine, and M. Yoshida, "Wearable photoplethysmographic sensors—Past and present," *Electronics*, vol. 3, no. 2, pp. 282–302, Apr. 2014.

[20] L. Cadmus-Bertram, R. Gangnon, E. J. Wirkus, K. M. Thraen-Borowski, and J. Gorzelitz-Liebhauser, "The accuracy of heart rate monitoring by some wrist-worn activity trackers," *Ann. Internal Med.*, vol. 166, no. 8, p. 610, Apr. 2017.

[21] E. Jo, K. Lewis, D. Directo, M. J. Kim, and B. A. Dolezal, "Validation of biofeedback wearables for photoplethysmographic heart rate tracking," *J. Sports Sci. Med.*, vol. 15, no. 3, p. 540, 2016.

[22] E. Rodriguez-Villegas, G. Chen, J. Radcliffe, and J. Duncan, "A pilot study of a wearable apnoea detection device," *Brit. Med. J. Open*, vol. 4, no. 10, p. 5299, 2014.

[23] I. Garcia-Lopez, P. Sharma, and E. Rodriguez-Villegas, "Heart rate extraction from novel neck photoplethysmography signals," in *Proc. 41st Annu. Int. Conf. IEEE Eng. Med. Biol. Soc. (EMBC)*, Jul. 2019, pp. 6541–6544.

[24] I. Garcia-Lopez and E. Rodriguez-Villegas, "Characterization of artifact signals in neck photoplethysmography," *IEEE Trans. Biomed. Eng.*, vol. 67, no. 10, pp. 2849–2861, Oct. 2020.

[25] M. Peng, S. A. Imtiaz, and E. Rodriguez-Villegas, "Pulse oximetry in the neck—A proof of concept," in *Proc. 39th Annu. Int. Conf. IEEE Eng. Med. Biol. Soc. (EMBC)*, Jul. 2017, pp. 877–880.

[26] I. Garcia-Lopez, S. A. Imtiaz, and E. Rodriguez-Villegas, "Characterization study of neck photoplethysmography," in *Proc. 40th Annu. Int. Conf. IEEE Eng. Med. Biol. Soc. (EMBC)*, Jul. 2018, pp. 4355–4358.

[27] Y. Zhong, Y. Pan, L. Zhang, and K.-T. Cheng, "A wearable signal acquisition system for physiological signs including throat PPG," in *Proc. 38th Annu. Int. Conf. IEEE Eng. Med. Biol. Soc. (EMBC)*, Aug. 2016, pp. 603–606.

[28] *High-Sensitivity Pulse Oximeter and Heart-Rate Sensor for Wearable Health MAX 30102 Datasheet*, Maxim Integr., San Jose, CA, USA, Oct. 2018.

[29] *LIS2DH12: MEMS Digital Output Motion Sensor Ultra-Low-Power High-Performance 3-Axis Nano Accelerometer LIS2DH12 Datasheet*, ST Microelectron., Geneva, Switzerland, Jul. 2017.

[30] *nRF52832 Product Specification V1.3, nRF52832 Datasheet*, Nordic Semicond., Trondheim, Norway, Feb. 2017.
[31] *Medical Information—Ultrabreathe*. Accessed: Jan. 3, 2021. [Online]. Available: https: //www.ultrabreathe.com/medical-information/
[32] J. Shin and J. Cho, "Noise-robust heart rate estimation algorithm from photoplethysmography signal with low computational complexity," *J. Healthcare Eng.*, vol. 2019, pp. 1–7, May 2019.
[33] H.-E. Liao, "Two discrete oscillator based adaptive notch filters (OSC ANFs) for noisy sinusoids," *IEEE Trans. Signal Process.*, vol. 53, no. 2, pp. 528–538, Feb. 2005.
[34] *Application Note 6845 Guidelines for SPO2 Measurement Using the Maxim? MAX32664 Sensor hub*, M. I. Products, San Jose, CA, USA, 2019.
[35] *Pulse Oximeters Premarket Notification Submissions [510(k)s]: Guidance for Industry and Food and Drug Administration Staff*, US Food and D. A. (FDA), Silver Spring, MD, USA, 2013.
[36] H. J. Davies, I. Williams, N. S. Peters, and D. P. Mandic, "In-ear SpO_2: A tool for wearable, unobtrusive monitoring of core blood oxygen saturation," *Sensors*, vol. 20, no. 17, p. 4879, Aug. 2020.
[37] B. Bradke and B. Everman, "Investigation of photoplethysmography behind the ear for pulse oximetry in hypoxic conditions with a novel device (SPYDR)," *Biosensors*, vol. 10, no. 4, p. 34, Apr. 2020.
[38] Y. Zhang *et al.*, "Motion artifact reduction for wrist-worn photoplethysmograph sensors based on different wavelengths," *Sensors*, vol. 19, no. 3, p. 673, Feb. 2019.
[39] J. Lee, M. Kim, H. K. Park, and I. Y. Kim, "Motion artifact reduction in wearable photoplethysmography based on multi-channel sensors with multiple wavelengths," *Sensors*, vol. 20, no. 5, p. 1493, 2020.
[40] J.-J. Liao, S.-Y. Chuang, C.-C. Chou, C.-C. Chang, and W.-C. Fang, "An effective photoplethysmography signal processing system based on EEMD method," in *Proc. VLSI Design, Automat. Test (VLSI-DAT)*, Apr. 2015, pp. 1–4.
[41] P. Thamarai and K. Adalarasu, "Denoising of EEG, ECG and PPG signals using Wavelet Transform," *J. Pharmaceutical Sci. Res.*, vol. 10, no. 1, pp. 156–161, 2018.
[42] *Toolkit for Commissioning and Planning Local NHS Services in the U.K. Obstructive Sleep Apnoea (OSA)*, Brit. Lung Found., London, U.K., 2015.
[43] M. Chu *et al.*, "Respiration rate and volume measurements using wearable strain sensors," *Npj Digit. Med.*, vol. 2, no. 1, pp. 1–9, 2019.

Sukhpreet Singh received the B.Eng. degree in biomedical engineering from the University of Victoria, Victoria, BC, Canada, in 2011.

His past experiences have included the development of upper limb prostheses and wearable device development for medical applications. He is currently a Research Assistant with the Wearable Technologies Laboratory, Imperial College London, London, U.K. His current interests include low-power electronics and optomechanical design optimization.

Michał Kozłowski received the M.Eng. and Ph.D. degrees from the University of Bristol, Bristol, U.K., in 2015 and 2020, respectively. His doctoral thesis addressed robust and efficient algorithms for indoor localization in healthcare applications.

He is currently a Research Associate with Imperial College London, London, U.K. His work spans the areas of machine learning, signal processing, robotics, wireless communications, and wearable sensor design. His current research interests include active learning, robustification of personal sensing systems, as well as efficient and practical data collection techniques.

Irene García-López (Student Member, IEEE) received the B.Eng. degree in biomedical engineering from the University Carlos III Madrid, Spain, in 2015, and the M.Sc. degree in neurotechnology from Imperial College London, London, U.K., in 2016, where she is currently pursuing the Ph.D. degree, focusing on signal processing of photoplethysmography signals.

Zhou Jiang received the B.Eng. degree in electrical and electronic engineering from the University of Bristol, Bristol, U.K., in 2011, the M.Sc. degree in integrated circuit design from Imperial College London, London, U.K., in 2012, and the Ph.D. degree from the Circuit sand Systems Group, Imperial College London, in 2017.

His current research interests include analog and digital integrated circuit designs for miniature wireless neuronal activity recording systems, ultralow power analogs, RF integrated circuit designs for wireless applications, and system level design with wireless wearable devices for recording vital physiological signals and health monitoring.

Esther Rodriguez-Villegas (Senior Member, IEEE) received the Ph.D. degree from the University of Seville, Seville, Spain, in 2002.

Since 2002, she has been a Faculty Member with the Imperial College London, London, U.K. Since 2015, she holds the Chair of low-power electronics with the Department of Electrical and Electronic Engineering. She is also the Director of the Wearable Technologies Laboratory. She has trained over 700 engineers from all over the world at the M.S. or Ph.D. levels in ultralow-power electronic design. She is also the Chief Scientific Officer of TaniTec, Ltd., London, and the Co-Chief Executive Officer of Acurable, Ltd., London, which she founded.

Dr. Rodriguez-Villegas has received a number of awards and honors, including being recognized as the Top Young Scientist/Engineer in Spain, in 2009 (the Complutense Award); the Institution of Engineering and Technology (U.K.) Innovation Award, in 2009; being recognized twice by the European Research Council as a Research Leader in Europe (Starting and Consolidator Awards, in 2010 and 2016); and the XPRIZE (USA) Award, in 2014.